Frontiers of Information Technology & Electronic Engineering
www.jzus.zju.edu.cn; engineering.cae.cn; www.springerlink.com
ISSN 2095-9184 (print); ISSN 2095-9230 (online)
E-mail: jzus@zju.edu.cn

Max-min rate optimization for multi-user MISO-OFDM systems assisted by RIS with a wideband model*

Yonghua QUAN[†1], Zhong TIAN[†‡1], Zhengchuan CHEN[†‡1,2], Min WANG[3,4], Yunjian JIA[1]

[1]*School of Microelectronics and Communication Engineering, Chongqing University, Chongqing 400044, China*

[2]*Shaanxi Key Laboratory of Information Communication Network and Security, Xi'an University of Posts & Telecommunications, Xi'an 710121, China*

[3]*School of Optoelectronic Engineering, Chongqing University of Posts and Telecommunications, Chongqing 400065, China*

[4]*Guangxi Wireless Broadband Communication and Signal Processing Key Laboratory, Guilin University of Electronic Technology, Guilin 541004, China*

[†]E-mail: qyh@cqu.edu.cn; ztian@cqu.edu.cn; czc@cqu.edu.cn

Received Feb. 27, 2023; Revision accepted Aug. 12, 2023; Crosschecked Dec. 1, 2023

Abstract: Reconfigurable intelligent surfaces (RISs) have the capability to change the wireless environment smartly. Considering the attenuation of subchannels and crowding users involved in the wideband system, we introduce RISs into the multi-user multi-input single-output (MU-MISO) system with orthogonal frequency division multiplexing (OFDM) for performance enhancement. Maximizing the minimum rate of dense users in an MU-MISO-OFDM system assisted by RIS with an approximate practical model is formulated as the joint optimization problem involving subcarrier allocation, transmit precoding (TPC) matrices at the base station, and RIS passive beamforming. A coalition-game subcarrier allocation (CSA) algorithm is proposed to solve space–frequency resource allocation on subcarriers, which reforms the interference topology among dense users. Fractional programming and convex optimization method are used to optimize the TPC matrices and the RIS passive beamforming, which improves the spectral efficiency synthetically across all subchannels in the wideband system. Simulation results indicate that the CSA algorithm provides a significant gain for dense users. Besides, the proposed joint optimization method shows the considerable advantage of the RISs in the MU-MISO-OFDM system.

Key words: Reconfigurable intelligent surface; Max-min rate; Coalition-game subcarrier allocation
https://doi.org/10.1631/FITEE.2300120 **CLC number:** TN929.5

1 Introduction

Wireless networks in the future, namely sixth generation (6G) networks, are expected to satisfy diverse requirements in terms of the quality of service and high data rate (Yang P et al., 2019; Liu et al., 2021). To achieve these goals, several enabling wireless technologies have been proposed in recent years, such as ultra-dense networks, massive multi-input multi-output (MIMO), and millimeter wave (mmWave) technology. Multi-input single-output systems with orthogonal frequency division

‡ Corresponding authors

* Project supported by the Graduate Research and Innovation Foundation of Chongqing, China (No. CYB23050), the National Natural Science Foundation of China (Nos. 62271092 and 62001074), the Fundamental Research Funds for the Central Universities, China (No. 2023CDJXY-037), the China Postdoctoral Science Foundation (No. 2022M710534), the Natural Science Foundation of Chongqing, China (Nos. CSTB2023NSCQ-MSX0933 and CSTB2022NSCQMSX0327), the Open Fund of the Shaanxi Key Laboratory of Information Communication Network and Security, China (No. ICNS202201), and the Opening Project of the Guangxi Wireless Broadband Communication and Signal Processing Key Laboratory, China (No. GXKL06230206)

ORCID: Yonghua QUAN, https://orcid.org/0000-0002-6181-496X; Zhong TIAN, https://orcid.org/0000-0003-3176-7290; Zhengchuan CHEN, https://orcid.org/0000-0002-2289-5621

multiplexing (MISO-OFDM) are used to serve multiple users simultaneously, jointly considering the freedoms in the frequency domain and spatial domain. Since the MISO-OFDM system encounters the characteristic of wideband frequency selectivity, the attenuation of subchannels would decrease the transmission rate and degrade the performance of the system. Besides, subcarrier allocation and transmit precoding (TPC) of multiple antennas at the base station (BS) would become an urgent challenge as the number of users in 6G networks becomes larger. All these problems call for emerging technologies and promising solutions.

Recently, reconfigurable intelligent surfaces (RISs), also known as intelligent reflecting surfaces, have drawn a lot of attention from researchers for their potential advantages in manipulating the radio environments of wireless channels with programmable devices. RISs have numerous passive elements, which can adjust the amplitude and phase shifts (Huang CW et al., 2019; Dai et al., 2020; di Renzo et al., 2020; ElMossallamy et al., 2020; Cao et al., 2021c; Tian et al., 2022). In recent years, the potential advantages of RISs have motivated some research on the joint application of RISs and other communication technologies, e.g., non-orthogonal multiple access (NOMA) (Hou et al., 2020a, 2020b), OFDM (Lin et al., 2020; Yang YF et al., 2020), MIMO (Huang CW et al., 2020a; You et al., 2021; Cui et al., 2023), physical layer security (Chen J et al., 2019), deep reinforcement learning (Huang CW et al., 2020b), multi-task learning (Cao et al., 2021b), and artificial intelligence (Cao et al., 2021a).

Most existing studies focus on the wireless communication system in the narrowband channels, while a few focus on the wideband frequency selective channels. In the research on the wideband system, Yang YF et al. (2020) studied the point-to-point OFDM system through the joint design of power allocation and RIS passive beamforming. Zhang and Zhang (2020) studied the maximization of channel capacity in RIS-aided point-to-point MIMO-OFDM systems. Note that some works (Yang YF et al., 2020; Zhang and Zhang, 2020) are based on an ideal RIS model, in which each element has a limited amplitude and an unlimited phase shift. Each RIS element responds equally to the wideband signal for all subcarriers. Thus, the design of RISs for this ideal model can be easily realized by successive convex approximation (SCA) (Marks and Wright, 1978), semidefinite relaxation (SDR) (Luo et al., 2010), majorization minimization (MM) (Sun et al., 2017), etc. However, the practical design of RISs renders it challenging to achieve an ideal response. In practice, each RIS element has different response characteristics corresponding to the incident signal of varying frequencies due to the limitation of hardware circuit (Smith et al., 2017; Tang et al., 2020). The design of such practical RIS models is often complex, leading to performance gaps between the practical and ideal RIS models. Based on the practical RIS model, Li HY et al. (2021) described the relationship between RIS phase shift and amplitude in the wideband system and designed a RIS-simplified practical model to maximize the rate by optimizing both power allocation and RIS passive beamforming. According to the frequency selection characteristics of RIS, Cai et al. (2022) skillfully designed a simple model with frequency band division to weaken the response difference of wideband incident signals to RIS.

In mmWave or terahertz frequency bands, beam squinting effect is a typical phenomenon, whereby the wideband signals sent by array antennas are sensitive to propagation delay, providing different received signals in the frequency domain for the same transmitted data symbols (Jian et al., 2019). The beam squinting effect usually appears for large bandwidth (1 GHz and above) and high carrier frequency (60 GHz and above) (Jian et al., 2019; Li ZR et al., 2023). In this work, the wideband refers to the bandwidth in the conventional frequency band (sub-6 GHz), e.g., 10 MHz bandwidth at the 2.4 GHz carrier frequency band. The response of the RIS practical model for the input signals in different frequency sub-carriers is non-uniform (Li HY et al., 2021). We focus mainly on optimizing the max-min rate for multi-user (MU) MISO-OFDM systems with the practical RIS model (It is interesting to jointly consider the beam squinting effect and the practical RIS model in our future work).

In the above research works on MU RIS-aided systems, most are aimed at sum-rate maximization, which is mainly to coordinate interference or resource competition among each user. RIS's flexible control of the wireless channel environment makes it better to deal with the problem of interference suppression. Note that in the problem of

sum-rate maximization, it is difficult to guarantee the rate requirement of each user. Adding user rate constraints as in Gao et al. (2020) allows users to meet the minimum rate requirements. This design may result in a sizeable sum-rate loss for an unacceptable or unreasonable setting. To handle the difficulty of sum-rate maximization, we can consider user fairness as much as possible, usually by setting up max-min problems (Zhao, 2019; Gao et al., 2020; Zheng et al., 2021; Esmaeili et al., 2022). In the max-min problem, BS power allocation and RIS passive beamforming can be obtained by the alternate optimization (AO) method. By fixing RIS passive beamforming, the transmission power of the BS can be expressed as second-order-cone programming (SOCP) to obtain the optimal solution. The optimization of RISs is more easily solved by using optimization tools, such as SDR and SCA methods. This kind of method may not be suitable for RIS-aided MU wideband systems due to the design of the practical RIS model. Considering the coupling of users, the design of algorithms has been very complex. The design of the practical RIS model makes the max-min problem more challenging to solve.

In this paper, considering user fairness, we focus on the problem of maximizing the minimum rate of dense users for MU-MISO-OFDM downlink communication assisted by RIS with an approximate practical model. Our contributions are as follows:

First, we study the joint design of TPC matrices and RIS passive beamforming with subcarrier allocation to maximize the minimum rate of dense users with an approximate practical RIS model. Aiming at addressing the challenges that RIS passive beamforming needs to accommodate the fairness of dense users at all subcarriers and subcarrier allocation, we propose a novel AO framework.

Second, we propose a coalition-game algorithm to allocate subcarriers for dense users, which can decouple subcarrier allocation from other optimized variables. The proposed algorithm can effectively improve inter-user interference by spatial projection. The subcarrier allocation algorithm between users and the RIS is proposed to improve the minimum rate of dense users.

Third, we design TPC matrices and RIS passive beamforming based on the fractional programming (FP) method. The overall problem is transformed into several subproblems, which can be solved by AO to obtain a locally optimal solution. When RIS passive beamforming is given by the approximate practical RIS model, TPC matrices are solved by SOCP. With fixed TPC matrices, RIS passive beamforming is solved by the penalty dual decomposition (PDD) method based on an approximate practical RIS model.

Notations: $\mathbb{E}[\cdot]$ denotes statistical expectation. $(\cdot)^*$, $(\cdot)^{\mathrm{T}}$, $(\cdot)^{\mathrm{H}}$, and $(\cdot)^{-1}$ denote the conjugate, transpose, conjugate-transpose, and inverse operations, respectively. $\mathcal{CN}\left(\mu,\sigma^2\right)$ denotes the distribution of a circularly symmetric complex Gaussian random variable with mean μ and variance σ^2. $|x|$ denotes the absolute value of a complex number x, and $\|\boldsymbol{w}\|_2$ the Euclidean norm of a vector $\boldsymbol{w}$; $\boldsymbol{I}_N$ indicates an $N\times N$ identity matrix; $\otimes$ denotes the Kronecker product; $\Re\{\cdot\}$ denotes the real part of a complex number. diag$(\cdot)$ and blkdiag$(\cdot)$ are diagonalization operation and operation of the block diagonal matrix, respectively.

2 System model

2.1 Response model of passive RISs

A passive RIS is composed of a large number of passive elements, each of which can provide diverse reflection patterns to change the incident signal. Each passive RIS element with an impedance adjustable circuit contains a set of reflection metallic patches, a varactor diode, and a dielectric substrate, and adjusts the reflection response, such as amplitude and phase shift (Chen WC et al., 2020; Wu and Zhang, 2020). The response of the RIS element is modeled as a parallel resonant circuit. Therefore, the response of RIS is affected by the frequency of the input signal. While the practical RIS model is complex, the coefficients of the RIS element can be approximated well by the simplified function (Cai et al., 2020; Li HY et al., 2021). Assuming that the central frequency of a wideband system is f_{c}, we set the reference phase shift (RPS) θ of a RIS element as the phase shift of the central frequency f_{c}. Define ϕ as the response coefficient of each RIS element. By defining the frequency of the signal f, based on the approximate practical RIS model, we have

$$\phi = A(\theta,f)\mathrm{e}^{\mathrm{j}B(\theta,f)}, \tag{1}$$

where $A(\theta,f)$ and $B(\theta,f)$ are defined as the amplitude and the phase shift for the incident signal of

frequency f (in GHz), respectively. We note that $A(\theta, f)$ and $B(\theta, f)$ are the functions of θ and f mapped to the amplitude and phase shift, respectively. The functions $A(\theta, f)$ and $B(\theta, f)$ are set by accurately approximating a practical RIS model of Li HY et al. (2021). Unlike the ideal RIS model in a narrowband system, we further use this approximate practical RIS model to build the cascaded channels between the BS and the users.

2.2 Channel model

As shown in Fig. 1, we consider a RIS-aided MU-MISO-OFDM downlink communication system. Assume that the BS configured with N_t antennas transmits data to K single-antenna users assisted by the RIS composed of M reflecting elements. There are N resource blocks in the frequency domain, where each resource block in the flat-fading subchannel includes a typical subcarrier for the explanation of simplicity. The sets of all subcarriers, users, and elements of the RIS are defined as $\mathcal{N} = \{1, 2, ..., N\}$, $\mathcal{K} = \{1, 2, ..., K\}$, and $\mathcal{M} = \{1, 2, ..., M\}$, respectively. Similar to Chen J et al. (2019) and Zhang and Zhang (2020), we consider perfect channel state information (CSI) as known instantaneously at the BS and RIS.

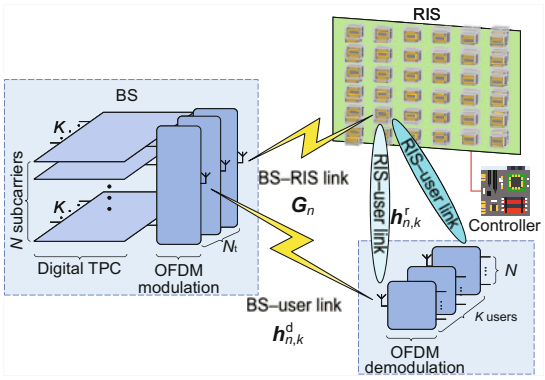

Fig. 1 A RIS-aided MU-MISO-OFDM downlink communication system

We define $\boldsymbol{h}^\mathrm{d}_{n,k} \in \mathbb{C}^{N_\mathrm{t}\times 1}$ as the channel response of the BS–user link in the frequency domain at the n^th subcarrier for the k^th user, which can be transformed from the corresponding channel response of the time domain in the wideband system (Zhang and Zhang, 2020). Similarly, the channel response of the RIS–user link at the n^th subcarrier for the k^th user in the frequency domain is denoted by $\boldsymbol{h}^\mathrm{r}_{n,k} \in \mathbb{C}^{M\times 1}$. Besides, the channel response of the BS–RIS link at the n^th subcarrier is given by $\boldsymbol{G}_n \in \mathbb{C}^{M\times N_\mathrm{t}}$. Let $\boldsymbol{\Phi}_n = \mathrm{diag}(\phi_{n,1}, \phi_{n,2}, \ldots, \phi_{n,M}) \in \mathbb{C}^{M\times M}, \forall n \in \mathcal{N}$ denote an equivalent diagonal matrix of RIS passive beamforming at the n^th subcarrier, where $\phi_{n,m}$ is given by

$$\phi_{n,m} = g(\theta_m, f_n), \forall n \in \mathcal{N}, \forall m \in \mathcal{M}. \tag{2}$$

In Eq. (2), $g(\theta_m, f_n)$ is a RIS response function of θ_m and f_n introduced by Eq. (1), where θ_m is defined as the RPS of the m^th RIS element; $f_n = f_\mathrm{c} + (n - \frac{N+1}{2})\frac{B}{N}$ is given by the central frequency of the n^th subcarrier with the system bandwidth B.

Then, the equivalent frequency-domain channels are expressed as follows:

$$\boldsymbol{h}^\mathrm{H}_{n,k} = (\boldsymbol{h}^\mathrm{d}_{n,k})^\mathrm{H} + (\boldsymbol{h}^\mathrm{r}_{n,k})^\mathrm{H}\boldsymbol{\Phi}_n\boldsymbol{G}_n, \forall n \in \mathcal{N}, \forall k \in \mathcal{K}. \tag{3}$$

The received signal of the n^th subcarrier for the k^th user is given by

$$\begin{aligned} y_{n,k} &= \boldsymbol{h}^\mathrm{H}_{n,k}\boldsymbol{W}_n\boldsymbol{s}_n + z_{n,k} \\ &= \boldsymbol{h}^\mathrm{H}_{n,k}\sum_{q=1}^{K}\boldsymbol{w}_{n,q}s_{n,q} + z_{n,k}, \end{aligned} \tag{4}$$

where $\boldsymbol{s}_n = [s_{n,1}, s_{n,2}, ..., s_{n,K}]^\mathrm{T} \in \mathbb{C}^{K\times 1}$ is the symbol vector at the n^th subcarrier transmitted to users, satisfying $\mathbb{E}[\boldsymbol{s}_n\boldsymbol{s}_n^\mathrm{H}] = \boldsymbol{I}_K, \forall n \in \mathcal{N}$. Then $\boldsymbol{W}_n = [\boldsymbol{w}_{n,1}, \boldsymbol{w}_{n,2}, ..., \boldsymbol{w}_{n,K}] \in \mathbb{C}^{N_\mathrm{t}\times K}$ is the TPC matrix of the n^th subcarrier, where $\boldsymbol{w}_{n,k} \in \mathbb{C}^{N_\mathrm{t}\times 1}$ is the TPC vector at the n^th subcarrier for the k^th user. $z_{n,k}$ is the additive white Gaussian noise (AWGN) of the n^th subcarrier for the k^th user with zero mean and noise variance σ^2, i.e., $z_{n,k} \sim \mathcal{CN}(0, \sigma^2)$. We consider that the noise of each user at each subcarrier is independent and identically distributed (i.i.d.). The signal-to-interference-plus-noise ratio (SINR) is thus expressed by

$$\gamma_{n,k} = \frac{c_{n,k}\left|\boldsymbol{h}^\mathrm{H}_{n,k}\boldsymbol{w}_{n,k}\right|^2}{\sum\limits_{q\neq k} c_{n,q}\left|\boldsymbol{h}^\mathrm{H}_{n,k}\boldsymbol{w}_{n,q}\right|^2 + \sigma^2}, \forall n \in \mathcal{N}, \forall k \in \mathcal{K}, \tag{5}$$

where $c_{n,k} = 1$ indicates that the n^th subcarrier is allocated to the k^th user; otherwise, $c_{n,k} = 0$. $\boldsymbol{C}$ is the matrix subcarrier allocation with each element, i.e., $[\boldsymbol{C}]_{n,k} = c_{n,k}$, $\forall n \in \mathcal{N}$, $\forall k \in \mathcal{K}$. Each user is allocated with at most one resource block, which implies $\sum_{n=1}^{N} c_{n,k} \leq 1, \forall k \in \mathcal{K}$.

2.3 Problem formulation

Considering user fairness, with R defined as the minimum rate of all users, the optimization problem of maximizing the minimum rate of users is given by

$$\begin{aligned}
\text{(P1)}\ & \max_{\boldsymbol{W},\boldsymbol{\theta},\boldsymbol{C},R} R \\
\text{s.t.}\ & \sum_{n=1}^{N}\log_2(1+\gamma_{n,k})\geq R,\ \forall k\in\mathcal{K}, && \text{(6a)}\\
& \sum_{n=1}^{N}\sum_{k=1}^{K} c_{n,k}\|\boldsymbol{w}_{n,k}\|_2^2\leq P, && \text{(6b)}\\
& \sum_{n=1}^{N} c_{n,k}\leq 1,\quad \forall k\in\mathcal{K}, && \text{(6c)}\\
& \sum_{k=1}^{K} c_{n,k}\leq K_n,\ \ \forall n\in\mathcal{N}, && \text{(6d)}\\
& c_{n,k}\in\{0,1\},\ \ \forall n\in\mathcal{N},\ \forall k\in\mathcal{K}, && \text{(6e)}\\
& \phi_{n,m}=g(\theta_m,f_n),\forall n\in\mathcal{N},\forall m\in\mathcal{M}, && \text{(6f)}
\end{aligned}$$

where $\boldsymbol{W}$, $\boldsymbol{\theta}$, P, and K_n are the collection of TPC matrices, the RPS vector of RIS, the total transmit power, and the maximum number of users permitted at the n^{th} subcarrier, respectively. Note that (P1) is a non-convex combinatorial optimization problem. In particular, (6e) is the non-convex binary constraint. The RIS passive beamforming $\boldsymbol{\Phi}$ is constrained by the non-convex nonlinear equality of $\boldsymbol{\theta}$ in (6f). Besides, the subcarrier allocation matrix $\boldsymbol{C}$, TPC matrices $\boldsymbol{W}$, and RIS passive beamforming $\boldsymbol{\Phi}$ are coupled in (6a). Therefore, it is challenging to derive the optimal solution of (P1) with polynomial system complexity. In the sequel, we propose an effective method to obtain a near-optimal solution for (P1).

3 Proposed solution

Since the max-min rate performance of dense users in the wideband system is determined by the couplings of multiple variables, i.e., $\boldsymbol{C}$, $\boldsymbol{W}$, and $\boldsymbol{\theta}$, our proposed solution adopts the AO framework to transform (P1) into several subproblems for optimizing each variable iteratively. Actually, subcarrier allocation has a vital impact on the interference topology among the users and the matching between the users and the selective subchannels in the wideband system. Besides, the passive beamforming of the RIS manipulates the selective subchannels in the wideband system synthetically, which can promote the rate performance of the users significantly.

For the subproblem of optimizing $\boldsymbol{C}$, we propose a coalition-game subcarrier allocation (CSA) algorithm. In addition, the joint design of TPC matrices and RIS passive beamforming obtains a suboptimal solution based on the non-convex block coordinate descent (BCD) method.

3.1 Subcarrier allocation algorithm design

The channel conditions of some subcarriers are probably suitable for multiple users. There is competition among users when considering subcarrier allocation. As the subproblem in (P1) about optimizing subcarrier allocation is binary integer non-linear programming, we propose the CSA algorithm of low complexity, which uses the channel gain and space correlation as the metrics. Considering the user channel condition as a metric, the coupling problem of (P1) for subcarrier allocation matrix $\boldsymbol{C}$ with other optimization variables $\boldsymbol{W}$ and $\boldsymbol{\theta}$ can be effectively solved.

Let $\mathcal{S}_n$ be the coalition of users for the n^{th} subcarrier. We have

$$c_{n,k}=\begin{cases}1,\ k\in\mathcal{S}_n,\\ 0,\ \text{otherwise.}\end{cases} \tag{7}$$

Let $|\mathcal{S}_n|$ be the number of users in the coalition for the n^{th} subcarrier. A disjoint coalition structure or coalition partition (Bogomolnaia and Jackson, 2002) is defined as $\Pi=\{\mathcal{S}_1,\mathcal{S}_2,...,\mathcal{S}_N\}$, satisfying $\cup_{n=1}^{N}\mathcal{S}_n=\mathcal{K}$, $|\mathcal{S}_n|\leq K_n$, $\mathcal{S}_i\cap\mathcal{S}_j=\varnothing$, $i\neq j$, $\forall i,\ j,\ n\in\mathcal{N}$, which are in accordance with (6c) and (6d). The utility function of each coalition is defined by the projected channel gains of the users in the complement space, shown as follows:

$$u(\mathcal{S}_n)=\sum\nolimits_{k\in\mathcal{S}_n}\left\|\boldsymbol{h}_k\hat{\boldsymbol{T}}_k\right\|_2^2, \tag{8}$$

where $\hat{\boldsymbol{T}}_k$ is the projection matrix (Tejera et al., 2006) given by Algorithm 1.

Given a current partition Π, let $\mathcal{S}_{\pi(i)}$ be the current coalition of user i. If we allow users between different coalitions to swap and form a swap pair (i,j), satisfying $\mathcal{S}_{\pi(i)}\neq\mathcal{S}_{\pi(j)}$, then the payoff function of (i,j) is defined as follows:

$$\begin{aligned}
r(i,j)=&u\left(\mathcal{S}_{\pi(i)}\backslash\{i\}\cup\{j\}\right)-u(\mathcal{S}_{\pi(i)})\\
&+u\left(\mathcal{S}_{\pi(j)}\backslash\{j\}\cup\{i\}\right)-u(\mathcal{S}_{\pi(j)}),
\end{aligned} \tag{9}$$

Algorithm 1 An assigned projection matrix

for $n=1$ **to** N **do**
  Initialize $t=0, \boldsymbol{T}_{(0)}=\boldsymbol{I}_{N_\mathrm{t}}$, and $\hat{\mathcal{S}}=\mathcal{S}_n$
  repeat
    Find $k=\arg\max_k \left\|\boldsymbol{h}_k\boldsymbol{T}_{(t)}\right\|_2^2,\ \forall k\in\hat{\mathcal{S}}$
    Set $\hat{\boldsymbol{T}}_k=\boldsymbol{T}_{(t)}$ and update $\hat{\mathcal{S}}=\hat{\mathcal{S}}\backslash\{k\}$
    Update $\boldsymbol{T}_{(t+1)}=\boldsymbol{T}_{(t)}-\frac{\boldsymbol{T}_{(t)}^{\mathrm{H}}\boldsymbol{h}_k^{\mathrm{H}}\boldsymbol{h}_k\boldsymbol{T}_{(t)}}{\left\|\boldsymbol{h}_k\boldsymbol{T}_{(t)}\right\|_2^2}, t=t+1$
  until $t\geq|S_n|$
end for

satisfying

$$\begin{cases} u(\mathcal{S}_{\pi(i)}\backslash\{i\}\cup\{j\})>u(\mathcal{S}_{\pi(i)}), \\ u(\mathcal{S}_{\pi(j)}\backslash\{j\}\cup\{i\})>u(\mathcal{S}_{\pi(j)}). \end{cases} \tag{10}$$

The swap condition in inequality (10) means that the allowed swap operation should not reduce the utility of the current coalitions.

Consequently, the proposed subcarrier allocation algorithm is designed by Algorithm 2. First, we divide the disjoint initial feasible partition Π_0 by giving $\boldsymbol{C}$ and $K_n, \forall n\in\mathcal{N}$ of all coalitions satisfying $\lceil K/N\rceil\geq K_n\geq\lfloor K/N\rfloor, \forall n\in\mathcal{N}$ and $\sum_{n=1}^N K_n=K$ with round-up operation $\lceil\cdot\rceil$ and round-down operation $\lfloor\cdot\rfloor$. Second, all the user pairs who meet the swap conditions in inequality (10) can perform a swap operation. For any user, the user is paired with another user in other coalitions to obtain the maximum payoff satisfying inequality (10) and swap their coalitions. The convergence of Algorithm 2 is guaranteed as follows:

Lemma 1 Given any initial user partition Π_0, the swap strategy of Algorithm 2 always converges to a final user partition Π_f composed of multiple disjoint coalitions.

Proof Algorithm 2 converges on the final partition Π_f if there is no swap pair satisfying inequality (10). According to swap pair $(i,j), \mathcal{S}_{\pi(i)}\neq\mathcal{S}_{\pi(j)}$, if $\exists(i,j)$, $u(\mathcal{S}_{\pi(i)}\backslash\{i\}\cup\{j\})>u(\mathcal{S}_{\pi(i)})$ and $u(\mathcal{S}_{\pi(j)}\backslash\{j\}\cup\{i\})>u(\mathcal{S}_{\pi(j)})$, it means that there is at least one swap pair to increase the utilities of the coalitions. Since a set has a finite number of partitions, only a limited number of swap pairs satisfy inequality (10). Therefore, the initial partition Π_0 eventually converges to a final partition Π_f.

3.2 TPC matrices and RIS beamforming

Given $\boldsymbol{C}$, due to the non-convexity of (P1) and the highly coupled nature of $\boldsymbol{W}$ and $\boldsymbol{\Phi}$ in inequality (6a), the optimization of $\boldsymbol{W},\boldsymbol{\theta}$ remains challenging. To deal with the sum of logarithms and the fraction in $\gamma_{n,k}$ in inequality (6a), motivated by the FP approach (Shen and Yu, 2018a), we transform (P1) into a more tractable form (P2). Let $\boldsymbol{\phi}_n=[\phi_{n,1},\phi_{n,2},\ldots,\phi_{n,M}]^{\mathrm{T}}$ define the RIS passive beamforming vector at the n^{th} subcarrier and $\boldsymbol{\phi}=\left[\boldsymbol{\phi}_1^{\mathrm{T}},\boldsymbol{\phi}_2^{\mathrm{T}},...,\boldsymbol{\phi}_N^{\mathrm{T}}\right]^{\mathrm{T}}$. Thus, (P1) is reformulated as follows:

$$\begin{aligned}(\mathrm{P2})\ &\max_{\boldsymbol{\alpha},\boldsymbol{\beta},\boldsymbol{\theta},\boldsymbol{W},R} R \\ &\text{s.t. } R_k(\boldsymbol{\alpha},\boldsymbol{\beta},\boldsymbol{\phi},\boldsymbol{W})\geq R,\ \forall k\in\mathcal{K}, \\ &\qquad (6\mathrm{b}),\ (6\mathrm{f}),\end{aligned} \tag{11}$$

where auxiliary variables $\boldsymbol{\alpha}$ and $\boldsymbol{\beta}$ are

$$\begin{aligned}\boldsymbol{\alpha}&=[\boldsymbol{\alpha}_1,\boldsymbol{\alpha}_2,...,\boldsymbol{\alpha}_N]^{\mathrm{T}},\\ \boldsymbol{\alpha}_n&=[\alpha_{n,1},\alpha_{n,2},...,\alpha_{n,K}]^{\mathrm{T}},\ \forall n\in\mathcal{N},\\ \boldsymbol{\beta}&=[\boldsymbol{\beta}_1,\boldsymbol{\beta}_2,...,\boldsymbol{\beta}_N]^{\mathrm{T}},\\ \boldsymbol{\beta}_n&=[\beta_{n,1},\beta_{n,2},...,\beta_{n,K}]^{\mathrm{T}},\ \forall n\in\mathcal{N}.\end{aligned}$$

Then, the rate $R_k(\boldsymbol{\alpha},\boldsymbol{\beta},\boldsymbol{\phi},\boldsymbol{W})$ of the k^{th} user is denoted by

$$\begin{aligned}R_k(\boldsymbol{\alpha},\boldsymbol{\beta},\boldsymbol{\phi},\boldsymbol{W})=&\sum_{n=1}^N\left(\log_2(1+\alpha_{n,k})-\alpha_{n,k}\right)\\ &+\sum_{n=1}^N 2\sqrt{c_{n,k}(1+\alpha_{n,k})}\Re\left\{\beta_{n,k}\tilde{\boldsymbol{h}}_{n,k}^{\mathrm{H}}\boldsymbol{w}_{n,k}\right\}\\ &-\sum_{n=1}^N|\beta_{n,k}|^2\left(\sum_{q=1}^K c_{n,q}\left|\tilde{\boldsymbol{h}}_{n,k}^{\mathrm{H}}\boldsymbol{w}_{n,q}\right|^2+\sigma^2\right),\end{aligned} \tag{12}$$

Algorithm 2 Coalition-game subcarrier allocation algorithm

Initialize Π_0 according to $\boldsymbol{C}$ and $K_n, \forall n\in\mathcal{N}$
Update $u(\mathcal{S}_n), \forall n\in\mathcal{N}$ by Eq. (8)
repeat
  For any user $i\in\mathcal{S}_{\pi(i)}$, try to find another user $j\in\mathcal{S}_{\pi(j)}$, $\mathcal{S}_{\pi(j)}\neq\mathcal{S}_{\pi(i)}$, to form a swap pair (i,j) satisfying inequality (10)
  Find greatest payoff function $r(i,j)$ as $r(i^\star,j^\star)$
  if $r(i^\star,j^\star)$ in inequality (10) **then**
    Update $\mathcal{S}_{\pi(i)}=\mathcal{S}_{\pi(i)}\backslash\{i\}\cup\{j\}$ and $\mathcal{S}_{\pi(j)}=\mathcal{S}_{\pi(j)}\backslash\{j\}\cup\{i\}$
    Update $u(\mathcal{S}_{\pi(i)})$ and $u(\mathcal{S}_{\pi(j)})$ by Eq. (8)
  end if
  Obtain current partition Π_c
until convergence to a stable final partition Π_f
Obtain the subcarrier allocation matrix $\boldsymbol{C}$ with Π_f
return subcarrier allocation matrix $\boldsymbol{C}$

where $\tilde{\boldsymbol{h}}_{n,k} = \boldsymbol{h}_{n,k}^{\mathrm{d}} + (\boldsymbol{H}_{n,k}^{\mathrm{r}})^{\mathrm{H}}\boldsymbol{\phi}_n^*$ with $\boldsymbol{H}_{n,k}^{\mathrm{r}} = \mathrm{diag}\left((\boldsymbol{h}_{n,k}^{\mathrm{r}})^{\mathrm{H}}\right)\boldsymbol{G}_n \in \mathbb{C}^{M\times N_{\mathrm{t}}}, \forall n \in \mathcal{N}, \forall k \in \mathcal{K}$.

One can iteratively update four variables $\boldsymbol{\alpha}, \boldsymbol{\beta}, \boldsymbol{\theta}$, and $\boldsymbol{W}$ to obtain a locally optimal solution of (P2) by the BCD method. The convergence of the BCD method and the equivalence between (P1) and (P2) are clarified in Shen and Yu (2018b) and Razaviyayn et al. (2013), respectively.

3.2.1 Optimization of auxiliary variables

By fixing TPC matrices $\boldsymbol{W}$, RPS vector $\boldsymbol{\theta}$, and auxiliary variable $\boldsymbol{\beta}$, the optimal $\boldsymbol{\alpha}$ can be given by solving (P2), i.e., $\partial R_k/\partial\alpha_{n,k} = 0, \forall n \in \mathcal{N}, \forall k \in \mathcal{K}$. Similarly, $\boldsymbol{\beta}$ is given by solving (P2). The optimal $\boldsymbol{\alpha}$ and $\boldsymbol{\beta}$ in (P2) can be obtained with some manipulations as follows:

$$\alpha_{n,k} = \frac{\zeta_{n,k}^2 + \zeta_{n,k}\sqrt{\zeta_{n,k}^2+4}}{2}, \tag{13}$$

$$\beta_{n,k} = \frac{\sqrt{c_{n,k}(1+\alpha_{n,k})}\tilde{\boldsymbol{h}}_{n,k}^{\mathrm{H}}\boldsymbol{w}_{n,k}}{\sum_{q=1}^{K} c_{n,q}\left|\tilde{\boldsymbol{h}}_{n,k}^{\mathrm{H}}\boldsymbol{w}_{n,q}\right|^2 + \sigma^2}, \tag{14}$$

where $\zeta_{n,k} = \sqrt{c_{n,k}}\Re\{\beta_{n,k}^*\tilde{\boldsymbol{h}}_{n,k}^{\mathrm{H}}\boldsymbol{w}_{n,k}\}$. Next, by reformulating (P2) as the following subproblems, let us optimize $\boldsymbol{W}$ and $\boldsymbol{\theta}$, respectively.

3.2.2 Optimization of TPC matrices

Given $\boldsymbol{\alpha}$, $\boldsymbol{\beta}$, and $\boldsymbol{\theta}$, the optimization problem of $\boldsymbol{W}$ and R is written by

$$\begin{aligned}(\mathrm{P2.1})\quad \max_{\boldsymbol{W},R}\quad & R\\ \text{s.t.}\quad & R_k^w(\boldsymbol{W}) \geq R, \quad \forall k \in \mathcal{K},\\ & \sum_{n=1}^{N}\sum_{k=1}^{K} c_{n,k}\|\boldsymbol{w}_{n,k}\|_2^2 \leq P,\end{aligned} \tag{15}$$

where $R_k^w(\boldsymbol{W})$ is

$$R_k^w(\boldsymbol{W}) = d_k^w + \Re\left\{2\boldsymbol{w}_k^{\mathrm{H}}\boldsymbol{f}_k^w\right\} - \sum_{n=1}^{N}\boldsymbol{w}_n^{\mathrm{H}}\boldsymbol{Q}_{n,k}^w\boldsymbol{w}_n, \tag{16}$$

where $\boldsymbol{w}_k = \left[\boldsymbol{w}_{1,k}^{\mathrm{T}}, \boldsymbol{w}_{2,k}^{\mathrm{T}}, ..., \boldsymbol{w}_{N,k}^{\mathrm{T}}\right]^{\mathrm{T}}, \forall k \in \mathcal{K}$ and $\boldsymbol{w}_n = \left[\boldsymbol{w}_{n,1}^{\mathrm{T}}, \boldsymbol{w}_{n,2}^{\mathrm{T}}, ..., \boldsymbol{w}_{n,K}^{\mathrm{T}}\right]^{\mathrm{T}}, \forall n \in \mathcal{N}$. $\boldsymbol{Q}_{n,k}^w$, $\boldsymbol{f}_k^w$, and d_k^w in Eq. (16) are given by

$$\boldsymbol{Q}_{n,k}^w = \mathrm{diag}(c_{n,1}, c_{n,2}, ..., c_{n,K}) \otimes \left(|\beta_{n,k}|^2\tilde{\boldsymbol{h}}_{n,k}\tilde{\boldsymbol{h}}_{n,k}^{\mathrm{H}}\right), \tag{17a}$$

$$\boldsymbol{f}_k^w = \left[\left(\boldsymbol{f}_{1,k}^w\right)^{\mathrm{T}}, \left(\boldsymbol{f}_{2,k}^w\right)^{\mathrm{T}}, ..., \left(\boldsymbol{f}_{N,k}^w\right)^{\mathrm{T}}\right]^{\mathrm{T}}, \tag{17b}$$

$$\boldsymbol{f}_{n,k}^w = \sqrt{c_{n,k}(1+\alpha_{n,k})}\beta_{n,k}\tilde{\boldsymbol{h}}_{n,k}, \tag{17c}$$

$$d_k^w = \sum_{n=1}^{N}\left(\log_2(1+\alpha_{n,k}) - \alpha_{n,k} - \sigma^2|\beta_{n,k}|^2\right). \tag{17d}$$

By observing $\boldsymbol{Q}_{n,k}^w$, $\forall n \in \mathcal{N}, k \in \mathcal{K}$ in (17a), it can be simply verified that the matrices are nonnegative semidefinite. Since (6b) and (15) are convex quadratic functions of the TPC matrices $\boldsymbol{W}$, (P2.1) is an SOCP problem. Thus, we adopt convex optimization tools (e.g., CVX (Grant and Boyd, 2014)) to solve (P2.1) for finding the optimal solution.

3.2.3 Optimization of RIS passive beamforming

For the convenience of notations, the quadratic function for $\boldsymbol{\phi}$ in Eq. (12) can be specified as

$$R_k^{\phi}(\boldsymbol{\phi}) = d_k^{\phi} + 2\Re\{\boldsymbol{\phi}^{\mathrm{H}}\boldsymbol{f}_k^{\phi}\} - \boldsymbol{\phi}^{\mathrm{H}}\boldsymbol{Q}_k^{\phi}\boldsymbol{\phi}, \tag{18}$$

where $\boldsymbol{Q}_k^{\phi}$, $\boldsymbol{f}_k^{\phi}$, and d_k^{ϕ} are

$$\boldsymbol{Q}_k^{\phi} = \mathrm{blkdiag}\left(\boldsymbol{Q}_{1,k}^{\phi}, \boldsymbol{Q}_{2,k}^{\phi}, ..., \boldsymbol{Q}_{N,k}^{\phi}\right), \tag{19a}$$

$$\boldsymbol{Q}_{n,k}^{\phi} = |\beta_{n,k}|^2\left(\sum_{q=1}^{K} c_{n,q}\boldsymbol{a}_{n,k,q}\boldsymbol{a}_{n,k,q}^{\mathrm{H}}\right), \tag{19b}$$

$$\boldsymbol{f}_k^{\phi} = \left[\left(\boldsymbol{f}_{1,k}^{\phi}\right)^{\mathrm{T}}, \left(\boldsymbol{f}_{2,k}^{\phi}\right)^{\mathrm{T}}, ..., \left(\boldsymbol{f}_{N,k}^{\phi}\right)^{\mathrm{T}}\right]^{\mathrm{T}}, \tag{19c}$$

$$\begin{aligned}\boldsymbol{f}_{n,k}^{\phi} = {}& \sqrt{c_{n,k}(1+\alpha_{n,k})}\beta_{n,k}^*\boldsymbol{a}_{n,k,k}\\ & - |\beta_{n,k}|^2\sum_{q=1}^{K} c_{n,q}b_{n,k,q}^*\boldsymbol{a}_{n,k,q},\end{aligned} \tag{19d}$$

$$\begin{aligned}d_k = {}& \sum_{n=1}^{N}\left(\log_2(1+\alpha_{n,k}) - \alpha_{n,k} - |\beta_{n,k}|^2\sigma^2\right)\\ & + \sum_{n=1}^{N} 2\sqrt{c_{n,k}(1+\alpha_{n,k})}\Re\{\beta_{n,k}^* b_{n,k,k}\}\\ & - \sum_{n=1}^{N}|\beta_{n,k}|^2\sum_{q=1}^{K} c_{n,q}b_{n,k,q}^2,\end{aligned} \tag{19e}$$

with $\boldsymbol{a}_{n,k,q} = \boldsymbol{H}_{n,k}^{\mathrm{r}}\boldsymbol{w}_{n,q}$ and $b_{n,k,q} = (\boldsymbol{h}_{n,k}^{\mathrm{d}})^{\mathrm{H}}\boldsymbol{w}_{n,q}$.

Fixing $\boldsymbol{\alpha}, \boldsymbol{\beta}$, $\boldsymbol{W}$, and R, the optimization problem for $\boldsymbol{\theta}$ is shown as follows:

$$\begin{aligned}(\text{P2.2}) \ \ &\text{find } \boldsymbol{\theta}\\ &\text{s.t. } R_k^{\phi}(\boldsymbol{\phi}) \geq R, \quad \forall k \in \mathcal{K}, &(20a)\\ &\phi_{n,m} = g(\theta_m, f_n), \forall n \in \mathcal{N}, \forall m \in \mathcal{M}. &(20b)\end{aligned}$$

Since $\boldsymbol{Q}_k^{\phi}$, $\forall k \in \mathcal{K}$ in Eq. (19a) can also be proved to be non-negative semidefinite matrices, (20a) is the convex constraint. Obviously, the difficulty of solving (P2.2) lies in the non-convex nonlinear constraints (20b). Thus, we can adopt the existing methods (Boyd et al., 2011; Huang KJ and Sidiropoulos, 2016) to solve (P2.2), such as the PDD method (Shi and Hong, 2020). Using the PDD method, we decompose the equality constraints and inequality constraints in (P2.2) into two subproblems, which can be optimized iteratively until convergence. By introducing the dual variable $\boldsymbol{\lambda}$ corresponding to (20b) and penalty parameter ρ, the augmented Lagrange (AL) function can be given by

$$\mathcal{L}(\boldsymbol{\phi}, \boldsymbol{\theta}, \boldsymbol{f}, \boldsymbol{\lambda}) \triangleq \frac{1}{2\rho} \left\| \boldsymbol{\phi} - \boldsymbol{g}(\boldsymbol{\theta}, \boldsymbol{f}) + \rho\boldsymbol{\lambda} \right\|_2^2, \quad (21)$$

where $\boldsymbol{g} \in \mathbb{C}^{MN \times 1}$ is the total RIS response function. The frequency vector of the incident signal is defined as $\boldsymbol{f} = [f_1, f_2, ..., f_N]^{\mathrm{T}}$. Note that $\boldsymbol{f}$ is usually given in wideband systems. Thus, the AL subproblem for (P2.2) can be represented as

$$\begin{aligned}(\text{P2.2}') \ \ &\min_{\boldsymbol{\phi}, \boldsymbol{\theta}} \mathcal{L}(\boldsymbol{\phi}, \boldsymbol{\theta}, \boldsymbol{\lambda})\\ &\text{s.t. } R_k^{\phi}(\boldsymbol{\phi}) \geq R, \quad \forall k \in \mathcal{K}. &(22)\end{aligned}$$

In addition, we can find the replacement problem of (P2.2′) to accelerate the AO process, similar to Zhao (2019).

Therefore, (P2.2′) is replaced by (P2.2″) as follows to find the better $\boldsymbol{\theta}$:

$$\begin{aligned}(\text{P2.2}'') \ \ &\min_{\boldsymbol{\phi}, \boldsymbol{\theta}, \varphi} \mathfrak{g}(\boldsymbol{\phi}, \boldsymbol{\theta}, \varphi, \boldsymbol{\lambda})\\ &\text{s.t. } R_k^{\phi}(\boldsymbol{\phi}) \geq \varphi + R, \quad \forall k \in \mathcal{K}, &(23)\\ &\varphi \geq 0, &(24)\end{aligned}$$

where $\mathfrak{g}(\boldsymbol{\phi}, \boldsymbol{\theta}, \varphi, \boldsymbol{\lambda}) \triangleq \frac{1}{2\rho} \left\| \boldsymbol{\phi} - \boldsymbol{g}(\boldsymbol{\theta}) + \rho\boldsymbol{\lambda} \right\|_2^2 - \varphi$. The variable φ can be understood as the "rate residual." Therefore, the subproblem of $\boldsymbol{\phi}$ and φ for (P2.2″) can be reformulated as follows:

$$(\text{P2.2.1}) \ \min_{\boldsymbol{\phi}, \varphi} \mathfrak{g} \ \text{ s.t. } (23), (24). \quad (25)$$

Noticing that (P2.2.1) is also an SOCP problem for $\boldsymbol{\phi}$ and φ, one can use the convex optimization tools to seek for the optimal solution.

Then, by solving (P2.2″) with respect to $\boldsymbol{\theta}$, the simplified subproblem is given by

$$(\text{P2.2.2}) \ \min_{\boldsymbol{\theta}} \left\| \bar{\boldsymbol{\phi}} - \boldsymbol{g}(\boldsymbol{\theta}) \right\|_2^2, \quad (26)$$

where $\bar{\boldsymbol{\phi}} = \boldsymbol{\phi} + \rho\boldsymbol{\lambda}$. It can be observed that (P2.2.2) is a non-linear least-squares problem. This problem could be solved by the Levenberg–Marquardt (LM) algorithm (Moré, 1978). Based on the PDD method, we propose Algorithm 3 for (P2.2) to obtain the solution of $\boldsymbol{\theta}$. The convergence of Algorithm 3 can be proved (Shi and Hong, 2020). The description is omitted here.

Algorithm 3 Proposed update $\boldsymbol{\theta}$ for (P2.2)

Initialize $j = 0$, t, $\varepsilon_{\text{in}} > 0, \varepsilon_{\text{out}} > 0, \rho > 0$, $\mu \in (0, 1)$, and feasible $\boldsymbol{\phi}_{\text{out}}^{(0)}, \boldsymbol{\theta}_{\text{out}}^{(0)}, \boldsymbol{\lambda}_{\text{out}}^{(0)}$
repeat
  Set $i = 0$, $\boldsymbol{\phi}_{\text{in}}^{(i)} = \boldsymbol{\phi}_{\text{out}}^{(j)}$, and $\boldsymbol{\theta}_{\text{in}}^{(i)} = \boldsymbol{\theta}_{\text{out}}^{(j)}$
  repeat
    Update $\boldsymbol{\phi}_{\text{in}}^{(i+1)}$ via solving (P2.2.1), according to $\boldsymbol{\theta}_{\text{in}}^{(i)}$, $\boldsymbol{\lambda}_{\text{out}}^{(j)}$, and ρ
    Update $\boldsymbol{\theta}_{\text{in}}^{(i+1)}$ via solving (P2.2.2), according to $\boldsymbol{\phi}_{\text{in}}^{(i+1)}$
    Set $i = i + 1$
  until $\left| \left(\mathfrak{g}\left(\boldsymbol{\phi}_{\text{in}}^{(i)}\right) - \mathfrak{g}\left(\boldsymbol{\phi}_{\text{in}}^{(i-1)}\right) \right) / \mathfrak{g}\left(\boldsymbol{\phi}_{\text{in}}^{(i)}\right) \right| \leq \varepsilon_{\text{in}}$ or $i \geq t$
  Set $\boldsymbol{\phi}_{\text{out}}^{(j+1)} = \boldsymbol{\phi}_{\text{in}}^{(i)}$ and $\boldsymbol{\theta}_{\text{out}}^{(j+1)} = \boldsymbol{\theta}_{\text{in}}^{(i)}$
  Set $\boldsymbol{\lambda}_{\text{out}}^{(j+1)} = \boldsymbol{\lambda}_{\text{out}}^{(j)} + \frac{1}{\rho}\left(\boldsymbol{\phi}_{\text{out}}^{(j+1)} - \boldsymbol{g}\left(\boldsymbol{\theta}_{\text{out}}^{(j+1)}\right)\right)$
  Set $\rho \leftarrow \mu\rho$ and $j = j + 1$
until $\left\| \boldsymbol{\phi}_{\text{out}}^{(j)} - \boldsymbol{g}\left(\boldsymbol{\theta}_{\text{out}}^{(j)}\right) \right\|_{\infty} \leq \varepsilon_{\text{out}}$ or $j \geq t$
return $\boldsymbol{\theta} \leftarrow \boldsymbol{\theta}_{\text{out}}^{(j)}$

3.2.4 Overall algorithm for solving (P1)

Based on the AO framework, we propose an overall method, which iteratively optimizes the variables $\boldsymbol{C}$, $\boldsymbol{W}$, and $\boldsymbol{\theta}$ to obtain a locally optimal solution. This method is summarized as Algorithm 4, which uses the CSA algorithm for subcarrier allocation and designs TPC matrices and RIS passive beamforming based on the FP approach and convex optimization. Note that the convergence of optimizing $\boldsymbol{W}$ and $\boldsymbol{\theta}$ iteratively could be guaranteed by the principle of the BCD method. Besides, the validation of updating $\boldsymbol{C}$ through the CSA algorithm is verified by permitting the termination of the iteration

Algorithm 4 RIS-CSA iterative AO for solving (P1)

Input: $\boldsymbol{h}_{n,k}^{\mathrm{d}}, \forall n \in \mathcal{N}, \forall k \in \mathcal{K}, \boldsymbol{h}_{n,k}^{\mathrm{r}}, \forall n \in \mathcal{N}, \forall k \in \mathcal{K}, \boldsymbol{G}_n, \forall n \in \mathcal{N}, P, K, N, N_{\mathrm{t}}, M, \sigma^2$
Output: R
Initialize $\boldsymbol{\theta}^{(0)}$, $\boldsymbol{C}^{(0)}$, and $\boldsymbol{W}^{(0)}$ to feasible values and $t=0$
Initialize $\boldsymbol{\alpha}^{(0)}$ and $\boldsymbol{\beta}^{(0)}$ by Eqs. (13) and (14), respectively
repeat
  Set $t=t+1$
  Update $\boldsymbol{\theta}^{(t)}$ via Algorithm 3
  Update $\boldsymbol{C}^{(t)}$ via solving (P3)
  Set $\boldsymbol{W}^{(t)}$ to feasible values according to $\boldsymbol{C}^{(t)}$
  repeat
    Update $\boldsymbol{\alpha}^{(t)}$ and $\boldsymbol{\beta}^{(t)}$ with Eqs. (13) and (14), respectively
    Update $\boldsymbol{W}^{(t)}$ by solving (P2.1)
  until the objective value of (P2.1) converges
  Update the objective function value $R^{(t)}$
  if $R^{(t)} < R^{(t-1)}$ **then**
    Set $\boldsymbol{C}^{(t)} = \boldsymbol{C}^{(t-1)}$ and $\boldsymbol{W}^{(t)} = \boldsymbol{W}^{(t-1)}$
    Go to line 10
  end if
until the objective function value R converges

process if the max-min rate of the users decreases in the next iteration.

To clarify the performance gain of Algorithm 4, an upper bound of the rate in (P1) is derived by relaxing the domain of (6e) into the continuous interval $[0,1]$. Thus, a convex problem (P3) for $\boldsymbol{C}$ is given by

$$\begin{aligned}(\mathrm{P3})\quad \max_{\boldsymbol{C},R}\quad & R\\ \text{s.t.}\quad & c_{n,k}\in[0,1], \forall n\in\mathcal{N},\ \forall k\in\mathcal{K}, \quad (27)\\ & (11),\ (6\mathrm{b}),\ (6\mathrm{c}),\ (6\mathrm{d}).\end{aligned}$$

Solving (P3) provides an optimal solution of virtual subcarrier allocation for the users. Here, virtual subcarrier allocation refers to that a user may be allocated with $\varrho \in [0,1]$ subcarrier, e.g., 0.3, which is not always achievable in practical systems. Therefore, the rate derived from (P3) can be regarded only as an upper bound of (P1) for performance comparison. The procedures of attaining the upper bound of (P1) with virtual subcarrier allocation are summarized as Algorithm 5 (RIS-Slack). For the update of the RIS passive beamforming $\boldsymbol{\phi}$ in Algorithm 5, we further relax the constraints (6f) of RIS beamforming to $|\phi_{n,m}| \le 1, \forall n \in \mathcal{N}, \forall m \in \mathcal{M}$. The update of RIS passive beamforming via solving the relaxed

Algorithm 5 RIS-Slack for (P1) as the upper bound

Input: $\boldsymbol{h}_{n,k}^{\mathrm{d}}, \forall n \in \mathcal{N}, \forall k \in \mathcal{K}, \boldsymbol{h}_{n,k}^{\mathrm{r}}, \forall n \in \mathcal{N}, \forall k \in \mathcal{K}, \boldsymbol{G}_n, \forall n \in \mathcal{N}, P, K, N, N_{\mathrm{t}}, M, \sigma^2$
Output: R
Initialize $\boldsymbol{\phi}^{(0)}$, $\boldsymbol{C}^{(0)}$, and $\boldsymbol{W}^{(0)}$ to feasible values and $t=0$
Initialize $\boldsymbol{\alpha}^{(0)}$ and $\boldsymbol{\beta}^{(0)}$ by Eqs. (13) and (14), respectively
repeat
  Set $t=t+1$
  Update $\boldsymbol{\phi}^{(t)}$ via solving (P4)
  Update $\boldsymbol{C}^{(t)}$ via solving (P3)
  Update $\boldsymbol{W}^{(t)}$ via solving (P2.1)
  Update $\boldsymbol{\alpha}^{(t)}$ and $\boldsymbol{\beta}^{(t)}$ via Eqs. (13) and (14), respectively
until R converges

convex problem in Algorithm 5 is given by

$$\begin{aligned}(\mathrm{P4})\quad \max_{\boldsymbol{\phi},R}\quad & R\\ \text{s.t.}\quad & R_k^{\phi}(\boldsymbol{\phi}) \ge R, \quad \forall k\in\mathcal{K}, \quad (28\mathrm{a})\\ & |\phi_{n,m}| \le 1, \forall n\in\mathcal{N}, \forall m\in\mathcal{M}. \quad (28\mathrm{b})\end{aligned}$$

By solving (P4), we can obtain the optimal solution, which is much better than the solution of the same RIS passive beamforming at all subcarriers. On the upper bound of performance, the RIS passive beamforming for solving (P4) does not accord with the design of the practical RIS model (1).

3.2.5 Complexity analysis of the algorithms

We analyze the complexity of the proposed algorithms. As Algorithm 1 is scheduled in Algorithm 2, the complexity of the utility function for each coalition in Eq. (8) by Algorithm 1 is $\mathcal{O}(K/N)$. Moreover, the complexity of Algorithm 2 is given by $I_{\mathrm{A2}} = \mathcal{O}\left(I_1\left(K^3/N\right)\right)$ in the worst case, where I_1 is the required iteration number for convergence of the final partition Π_{f}. Although the subproblem for (P2.2.1) is an SOCP problem, we can solve it by methods such as the interior point method (IPM) (Lobo et al., 1998). In Algorithm 3, the complexity of solving (P2.2.1) is higher than that of solving (P2.2.2). Therefore, we have that the complexity of updating $\boldsymbol{\phi}$ for (P2.2.1) in each iteration is given by $\mathcal{O}\left(K^{1.5}M^3\right)$. We have $I_{\mathrm{A3}} = \mathcal{O}\left(I_2K^{1.5}M^3\right)$ as the complexity of Algorithm 3, where I_2 is the number of iterations required for the convergence for the inner and outer layers. The overall complexity of Algorithm 4 depends mainly on the updates

of two complex variables $\boldsymbol{W}$ and $\boldsymbol{\theta}$. The update of $\boldsymbol{\theta}$ is solved by Algorithm 3. Then, the complexity of solving (P2.1), which is an SOCP problem, is $\mathcal{O}\left(K^{3.5}N^2N_{\mathrm{t}}^2\right)$ in the worst case. Thus, the overall complexity of Algorithm 4 is given by $\mathcal{O}\left(I_3\left(I_4K^{3.5}N^2N_{\mathrm{t}}^2+I_{\mathrm{A2}}+I_{\mathrm{A3}}\right)\right)$, where I_3 and I_4 are the numbers of iterations required for convergence of variable R and solving (P2.1), respectively. Similarly, the complexity of solving (P3) is given by $I_5=\mathcal{O}\left((K+N)^{1.5}(KN)^2\right)$ by IPM in the worst case. The complexity of solving (P4) is $\mathcal{O}\left(K^{1.5}M^3\right)$ by IPM. Thus, the complexity of Algorithm 5 is given by $\mathcal{O}\left(I_6\left(I_5+K^{3.5}N^2N_{\mathrm{t}}^2+K^{1.5}M^3\right)\right)$, where I_6 defines the required iteration number for convergence.

4 Numerical results

In this section, simulation results are provided to demonstrate the max-min rate enhancement of the users achieved using our method. The BS and RIS are deployed at (0, 0) and (0, 50) m, respectively. Besides, K single-antenna users are randomly distributed in a circle with center (50, 5) m and radius $r=3$ m. Uniform linear arrays are deployed at the BS and RIS. The approximate practical model of RIS can be set up following Li HY et al. (2021). According to Zhang and Zhang (2020), all channels with Rician fading are configured as in Table 1. The time-domain channels of non-line-of-sight (NLOS) follow the distribution of $\mathcal{CN}(0,1/L)$. To illustrate the system performance of our proposed method (RIS-CSA) for dense users, the benchmark schemes are shown as follows:

1. RIS-RSA: With random subcarrier allocation (RSA) $\boldsymbol{C}$, optimize $\boldsymbol{W}$ and $\boldsymbol{\theta}$ by solving (P2.1) and Algorithm 3, respectively.

2. RPB-CSA: Given random passive beamforming (RPB) $\boldsymbol{\theta}$, $\boldsymbol{W}$ and $\boldsymbol{C}$ are optimized by solving (P2.1) and CSA, respectively.

3. RPB-RSA: Given $\boldsymbol{\theta}$ and $\boldsymbol{C}$ by random selection, optimize only $\boldsymbol{W}$ by solving (P2.1).

4. RIS-Slack: Relax the RIS approximation practical model and subcarrier allocation.

Algorithm 5 is used to obtain the max-min rate of the users as the upper bound.

As shown in Fig. 2, we offer the convergence behavior of different schemes. Except for the slow convergence of the RIS-Slack scheme, all other schemes can converge within 15 iterations. The minimum rate of users can quickly converge in the proposed AO algorithm. Fig. 3 shows the max-min rate of users in different schemes versus the total transmit power P. Since designing RIS passive beamforming provides more spatial diversity for dense users, the proposed RIS-aided schemes with CSA or RSA outperform the corresponding RPB schemes. As P goes up, our proposed RIS-CSA has moderate gain over the RIS-RSA scheme, where the users in the coalitions of CSA have highly spatially uncorrelated channels and high channel gains. Besides, the max-min rate of our proposed RIS-CSA method approaches the upper bound (RIS-Slack) closely.

Fig. 4 compares the minimum rate of users in different schemes versus the number of elements M on the RIS. As M increases, all RIS-aided schemes have a significant performance gain. When RIS passive beamforming is randomly initialized in RSA or CSA, the performance gain of deploying RIS is negligible. The performance gap between the proposed scheme and the RIS-Slack scheme increases with the increase of M because the phase and

Table 1 Channel environment parameters of RIS in wideband communication

Parameter	Value
Path loss exponent of the BS–RIS link	2.2
Path loss exponent of the RIS–user link	2.8
Path loss exponent of the BS–user link	3.5
Path loss of 1 m distance	−30 dB
Length of the OFDM cyclic prefix	8
Number of delayed taps	$L=2$
Number of allocated subcarriers	$N=5$
Rician factor of all channels	$\omega=10$
Carrier frequency	2.4 GHz
Transmission bandwidth	10 MHz
Noise power spectral density	−174 dBm/Hz

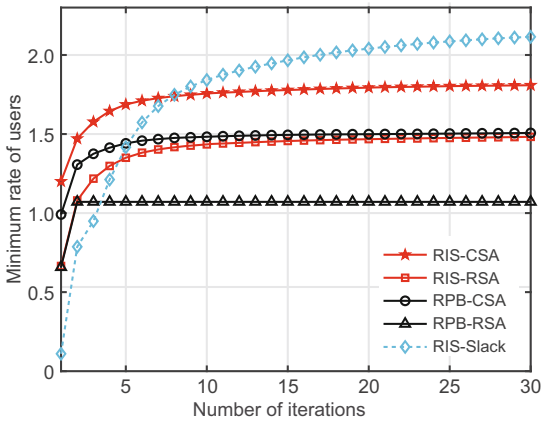

Fig. 2 Minimum rate of users versus the number of iterations with $K=15$, $P=10$ dBm, and $M=40$

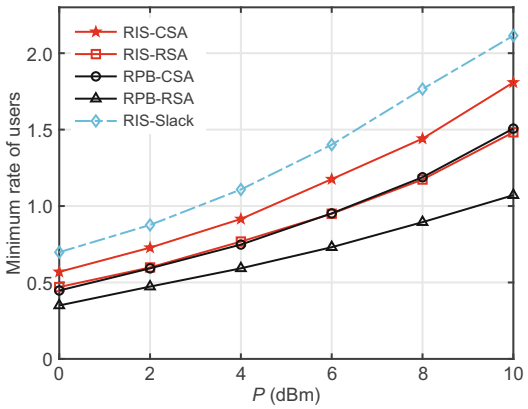

Fig. 3 Minimum rate of users versus P with $K = 15$ and $M = 40$

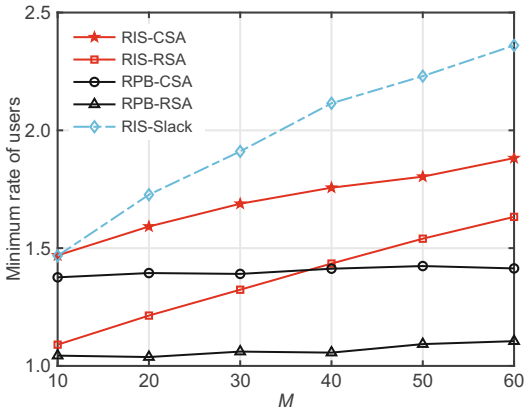

Fig. 4 Minimum rate of users versus M with $K = 15$ and $P = 10$ dBm

amplitude constraints of RISs under the practical RIS model are tighter than in the "ideal" RIS model of (P4).

As shown in Fig. 5, our proposed RIS-CSA scheme can use the remaining spatial degrees of freedom better to obtain a superior rate performance. As the number of users increases, the rate performance of the RPB-RSA scheme can be very close to that of the RIS-CSA or RIS-Slack scheme. When the number of users becomes too large, the spatial degrees of freedom are not enough, resulting in the degradation of the system performance. However, the optimized passive beamforming of RIS can still obtain good performance gain in the case of dense users. As observed in the region of dense users, e.g., K ranges from 15 to 25, the max-min rate gap between our proposed RIS-CSA scheme and the upper bound determined by RIS-Slack vanishes gradually, which means that the RIS-CSA scheme attains approximately the optimal solution.

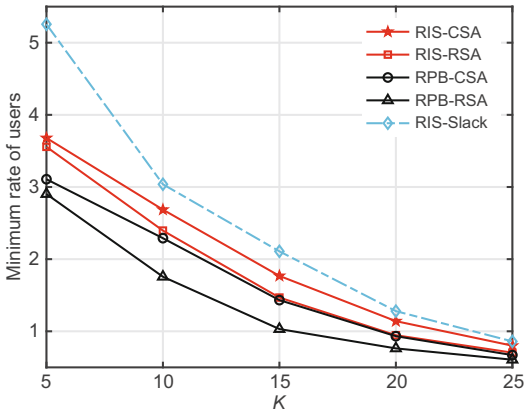

Fig. 5 Minimum rate of users versus K with $P = 10$ dBm and $M = 40$

5 Conclusions

We investigated an MU-MISO-OFDM downlink system assisted by RIS with an approximate practical model where the minimum rate of dense users is maximized. The joint design of subcarrier allocation, TPC matrices, and RIS passive beamforming was formulated to obtain a suboptimal solution. The spatial degrees of freedom in the system were improved by optimizing RIS passive beamforming. This indicated that deploying RIS simultaneously improves the spectral efficiency for all subcarriers while considering user fairness. The hybrid iterative AO method including CSA and RIS design provides a potential solution for max-min rate enhancement in the MU-MISO-OFDM system. The performance of the proposed algorithm was verified by simulations, showing that the RIS-aided wireless system has advantages over the proposed subcarrier allocation for dense users.

Contributors

Yonghua QUAN, Zhong TIAN, and Zhengchuan CHEN designed the research. Yonghua QUAN processed the data and drafted the paper. Zhong TIAN and Zhengchuan CHEN helped organize the paper. All authors revised and finalized the paper.

Compliance with ethics guidelines

Yonghua QUAN, Zhong TIAN, Zhengchuan CHEN, Min WANG, and Yunjian JIA declare that they have no conflict of interest.

Data availability

The data that support the findings of this study are available from the corresponding authors upon reasonable request.

References

Bogomolnaia A, Jackson MO, 2002. The stability of hedonic coalition structures. *Games Econ Behav*, 38(2):201-230. https://doi.org/10.1006/game.2001.0877

Boyd S, Parikh N, Chu E, et al., 2011. Distributed optimization and statistical learning via the alternating direction method of multipliers. *Found Trends Mach Learn*, 3(1):1-122. https://doi.org/10.1561/2200000016

Cai WH, Li HY, Li M, et al., 2020. Practical modeling and beamforming for intelligent reflecting surface aided wideband systems. *IEEE Commun Lett*, 24(7):1568-1571. https://doi.org/10.1109/LCOMM.2020.2987322

Cai WH, Liu R, Li M, et al., 2022. IRS-assisted multi-cell multiband systems: practical reflection model and joint beamforming design. *IEEE Trans Commun*, 70(6):3897-3911. https://doi.org/10.1109/TCOMM.2022.3168645

Cao XL, Yang B, Huang CW, et al., 2021a. AI-assisted MAC for reconfigurable intelligent-surface-aided wireless networks: challenges and opportunities. *IEEE Commun Mag*, 59(6):21-27. https://doi.org/10.1109/MCOM.001.2001146

Cao XL, Yang B, Huang CW, et al., 2021b. Reconfigurable-intelligent surface-assisted aerial-terrestrial communications via multi-task learning. *IEEE J Sel Areas Commun*, 39(10):3035-3050. https://doi.org/10.1109/JSAC.2021.3088634

Cao XL, Yang B, Zhang HL, et al., 2021c. Reconfigurable-intelligent-surface-assisted MAC for wireless networks: protocol design, analysis, and optimization. *IEEE Int Things J*, 8(18):14171-14186. https://doi.org/10.1109/JIOT.2021.3068492

Chen J, Liang YC, Pei YY, et al., 2019. Intelligent reflecting surface: a programmable wireless environment for physical layer security. *IEEE Access*, 7:82599-82612. https://doi.org/10.1109/ACCESS.2019.2924034

Chen WC, Bai L, Tang WK, et al., 2020. Angle-dependent phase shifter model for reconfigurable intelligent surfaces: does the angle-reciprocity hold? *IEEE Commun Lett*, 24(9):2060-2064. https://doi.org/10.1109/LCOMM.2020.2993961

Cui MY, Wu ZD, Lu Y, et al., 2023. Near-field MIMO communications for 6G: fundamentals, challenges, potentials, and future directions. *IEEE Commun Mag*, 61(1):40-46. https://doi.org/10.1109/MCOM.004.2200136

Dai LL, Wang BC, Wang M, et al., 2020. Reconfigurable intelligent surface-based wireless communications: antenna design, prototyping, and experimental results. *IEEE Access*, 8:45913-45923. https://doi.org/10.1109/ACCESS.2020.2977772

di Renzo M, Zappone A, Debbah M, et al., 2020. Smart radio environments empowered by reconfigurable intelligent surfaces: how it works, state of research, and the road ahead. *IEEE J Sel Areas Commun*, 38(11):2450-2525. https://doi.org/10.1109/JSAC.2020.3007211

ElMossallamy MA, Zhang HL, Song LY, et al., 2020. Reconfigurable intelligent surfaces for wireless communications: principles, challenges, and opportunities. *IEEE Trans Cogn Commun Netw*, 6(3):990-1002. https://doi.org/10.1109/Tccn.2020.2992604

Esmaeili H, Ahmad AA, Nadeem QUA, et al., 2022. Fairness analysis in IRS assisted C-RAN with imperfect CSI. IEEE Globecom Workshops, p.1010-1015. https://doi.org/10.1109/GCWkshps56602.2022.10008546

Gao YL, Yong C, Xiong ZH, et al., 2020. Reconfigurable intelligent surface for MISO systems with proportional rate constraints. IEEE Int Conf on Communications, p.1-7. https://doi.org/10.1109/ICC40277.2020.9148766

Grant M, Boyd S, 2014. CVX: Matlab Software for Disciplined Convex Programming. Version 2.1. Available from http://cvxr.com/cvx [Accessed on Feb. 1, 2023].

Hou TW, Liu YW, Song ZY, et al., 2020a. MIMO-NOMA networks relying on reconfigurable intelligent surface: a signal cancellation-based design. *IEEE Trans Commun*, 68(11):6932-6944. https://doi.org/10.1109/TCOMM.2020.3018179

Hou TW, Liu YW, Song ZY, et al., 2020b. Reconfigurable intelligent surface aided NOMA networks. *IEEE J Sel Areas Commun*, 38(11):2575-2588. https://doi.org/10.1109/JSAC.2020.3007039

Huang CW, Zappone A, Alexandropoulos GC, et al., 2019. Reconfigurable intelligent surfaces for energy efficiency in wireless communication. *IEEE Trans Wirel Commun*, 18(8):4157-4170. https://doi.org/10.1109/TWC.2019.2922609

Huang CW, Hu S, Alexandropoulos GC, et al., 2020a. Holographic MIMO surfaces for 6G wireless networks: opportunities, challenges, and trends. *IEEE Wirel Commun*, 27(5):118-125. https://doi.org/10.1109/MWC.001.1900534

Huang CW, Mo RH, Yuen C, 2020b. Reconfigurable intelligent surface assisted multiuser MISO systems exploiting deep reinforcement learning. *IEEE J Sel Areas Commun*, 38(8):1839-1850. https://doi.org/10.1109/JSAC.2020.3000835

Huang KJ, Sidiropoulos ND, 2016. Consensus-ADMM for general quadratically constrained quadratic programming. *IEEE Trans Signal Process*, 64(20):5297-5310. https://doi.org/10.1109/TSP.2016.2593681

Jian MN, Gao FF, Tian Z, et al., 2019. Angle-domain aided UL/DL channel estimation for wideband mmWave massive MIMO systems with beam squint. *IEEE Trans Wirel Commun*, 18(7):3515-3527. https://doi.org/10.1109/TWC.2019.2915072

Li HY, Cai WH, Liu Y, et al., 2021. Intelligent reflecting surface enhanced wideband MIMO-OFDM communications: from practical model to reflection optimization. *IEEE Trans Commun*, 69(7):4807-4820. https://doi.org/10.1109/TCOMM.2021.3069860

Li ZR, Gao Z, Li T, 2023. Sensing user's channel and location with terahertz extra-large reconfigurable intelligent surface under hybrid-field beam squint effect. *IEEE J Sel Top Signal Process*, 17(4):893-911. https://doi.org/10.1109/JSTSP.2023.3278942

Lin SE, Zheng BX, Alexandropoulos GC, et al., 2020. Adaptive transmission for reconfigurable intelligent surface-assisted OFDM wireless communications. *IEEE J Sel Areas Commun*, 38(11):2653-2665. https://doi.org/10.1109/JSAC.2020.3007038

Liu YW, Liu X, Mu XD, et al., 2021. Reconfigurable intelligent surfaces: principles and opportunities. *IEEE Commun Surv Tut*, 23(3):1546-1577. https://doi.org/10.1109/COMST.2021.3077737

Lobo MS, Vandenberghe L, Boyd S, et al., 1998. Applications of second-order cone programming. *Linear Algebra Appl*, 284(1-3):193-228. https://doi.org/10.1016/S0024-3795(98)10032-0

Luo ZQ, Ma WK, So AMC, et al., 2010. Semidefinite relaxation of quadratic optimization problems. *IEEE Signal Process Mag*, 27(3):20-34. https://doi.org/10.1109/Msp.2010.936019

Marks BR, Wright GP, 1978. Technical note—a general inner approximation algorithm for nonconvex mathematical programs. *Oper Res*, 26(4):681-683. https://doi.org/10.1287/opre.26.4.681

Moré JJ, 1978. The Levenberg-Marquardt algorithm: implementation and theory. Proc Biennial Conf on Numerical Analysis, p.105-116. https://doi.org/10.1007/BFb0067700

Razaviyayn M, Hong MY, Luo ZQ, 2013. A unified convergence analysis of block successive minimization methods for nonsmooth optimization. *SIAM J Optim*, 23(2):1126-1153. https://doi.org/10.1137/120891009

Shen KM, Yu W, 2018a. Fractional programming for communication systems—Part I: power control and beamforming. *IEEE Trans Signal Process*, 66(10):2616-2630. https://doi.org/10.1109/Tsp.2018.2812733

Shen KM, Yu W, 2018b. Fractional programming for communication systems—Part II: uplink scheduling via matching. *IEEE Trans Signal Process*, 66(10):2631-2644. https://doi.org/10.1109/TSP.2018.2812748

Shi QJ, Hong MY, 2020. Penalty dual decomposition method for nonsmooth nonconvex optimization—Part I: algorithms and convergence analysis. *IEEE Trans Signal Process*, 68:4108-4122. https://doi.org/10.1109/TSP.2020.3001906

Smith DR, Yurduseven O, Mancera LP, et al., 2017. Analysis of a waveguide-fed metasurface antenna. *Phys Rev Appl*, 8(5):054048. https://doi.org/10.1103/PhysRevApplied.8.054048

Sun Y, Babu P, Palomar DP, 2017. Majorization-minimization algorithms in signal processing, communications, and machine learning. *IEEE Trans Signal Process*, 65(3):794-816. https://doi.org/10.1109/tsp.2016.2601299

Tang WK, Dai JY, Chen MZ, et al., 2020. MIMO transmission through reconfigurable intelligent surface: system design, analysis, and implementation. *IEEE J Sel Areas Commun*, 38(11):2683-2699. https://doi.org/10.1109/JSAC.2020.3007055

Tejera P, Utschick W, Bauch G, et al., 2006. Subchannel allocation in multiuser multiple-input-multiple-output systems. *IEEE Trans Inform Theory*, 52(10):4721-4733. https://doi.org/10.1109/TIT.2006.881751

Tian Z, Chen ZC, Wang M, et al., 2022. Reconfigurable intelligent surface empowered optimization for spectrum sharing: scenarios and methods. *IEEE Veh Technol Mag*, 17(2):74-82. https://doi.org/10.1109/MVT.2022.3157070

Wu QQ, Zhang R, 2020. Towards smart and reconfigurable environment: intelligent reflecting surface aided wireless network. *IEEE Commun Mag*, 58(1):106-112. https://doi.org/10.1109/Mcom.001.1900107

Yang P, Xiao Y, Xiao M, et al., 2019. 6G wireless communications: vision and potential techniques. *IEEE Netw*, 33(4):70-75. https://doi.org/10.1109/MNET.2019.1800418

Yang YF, Zheng BX, Zhang SW, et al., 2020. Intelligent reflecting surface meets OFDM: protocol design and rate maximization. *IEEE Trans Commun*, 68(7):4522-4535. https://doi.org/10.1109/TCOMM.2020.2981458

You L, Xiong JY, Ng DWK, et al., 2021. Energy efficiency and spectral efficiency tradeoff in RIS-aided multiuser MIMO uplink transmission. *IEEE Trans Signal Process*, 69:1407-1421. https://doi.org/10.1109/TSP.2020.3047474

Zhang SW, Zhang R, 2020. Capacity characterization for intelligent reflecting surface aided MIMO communication. *IEEE J Sel Areas Commun*, 38(8):1823-1838. https://doi.org/10.1109/jsac.2020.3000814

Zhao J, 2019. Optimizations with intelligent reflecting surfaces (IRSs) in 6G wireless networks: power control, quality of service, max-min fair beamforming for unicast, broadcast, and multicast with multi-antenna mobile users and multiple IRSs. http://arxiv.org/abs/1908.03965

Zheng BX, You CS, Zhang R, 2021. Double-IRS assisted multi-user MIMO: cooperative passive beamforming design. *IEEE Trans Wirel Commun*, 20(7):4513-4526. https://doi.org/10.1109/Twc.2021.3059945